Synthesis of Fullerene- and Nanotube-Like SnS_2 Nanoparticles and Sn/S/Carbon Nanocomposites

Aswani Yella,[†] Enrico Mugnaioli,[†] Helen Annal Therese,[†] Martin Panthöfer,[†] Ute Kolb,[†] and Wolfgang Tremel*,[†]

Institut für Anorganische Chemie und Analytische Chemie der Johannes Gutenberg-Universität, Duesbergweg 10-14, D-55099 Mainz, Germany, and Institut für Physikalische Chemie der Johannes Gutenberg-Universität, Welderweg 11, Mainz, Germany

Received January 29, 2009. Revised Manuscript Received April 10, 2009

SnS_2 nested fullerene-type (IF) nanoparticles, nanotubes, and SnS_2/C hybrid nanostructures were obtained by vapor transport starting from elemental tin and CS_2. The reaction was carried out in a single-step process by heating elemental tin metal powder in a horizontal tube furnace at 800−1000 °C. TEM analysis allowed proposing a plausible mechanism for the formation of fullerene-like particles of SnS_2 as well as tubes and scrolls from nanosheets of SnS_2. Pure material could be obtained by optimizing the reaction based on a product analysis using powder X-ray diffraction (XRD) and high-resolution transmission electron microscopy (HRTEM) combined with energy-dispersive X-ray spectroscopy (EDX).

Introduction

Carbon fullerenes and nanotubes have engendered intense scientific interest because of their promising electronic and mechanical properties.[1−3] These findings have prompted efforts to develop simple and cheap methods for large-scale production of these materials. The propensity of graphite to form hollow closed structures is believed to stem from the high energy of dangling bonds at the edge of the graphene planes.[1−3] Because this is also true for other inorganic layered structures, the formation of closed caged nanoparticles is a general property of all materials with anisotropic layer-type structures. On the basis of this working hypothesis, numerous types of closed nanostructures from materials such as MoS_2,[4,5] $NiCl_2$,[6] or GaSe[7] have been synthesized. These materials have properties that make them promising for various optical, magnetic, electronic, and especially mechanical applications.

Although nested fullerenes, nanopolyhedra, and nanotubes represent an integral part of the phase diagram of MS_2,[8] they are metastable at room temperature. MS_2 fullerene-type nanoparticles and nanotubes are high-temperature and low-pressure phases in the M−S diagrams that are not accessible by traditional solid-state synthesis. In conventional high-temperature reactions, the energy required for solid-state diffusion of the reactants would exceed the nucleation energy of metastable MS_2 nanoparticles. As a consequence, only the thermodynamically stable crystalline products are formed. In contrast, reactions are kinetically controlled if solid-state diffusion plays only a minor role. Here a phase may nucleate and grow until its growth exhausts the supply of the reactants. Now the sequence of phases formed depends on the relative activation energies of nucleation.

Consequently, most reported synthetic approaches to nanoparticular MS_2 inorganic fullerenes (IF) and nanotubes (NT) are gas-phase reactions where highly mobile species are trapped kinetically. A very successful method for the preparation of metal chalcogenide nanoparticles is the reductive sulfidization of metal oxides with H_2S.[9,10] This approach has been restricted so far to transition metals such as V,[11] Mo,[12] W,[13] and Re,[14] i.e., for those metals where the

* Corresponding author. Tel: (49) 6131-39-25135. Fax: (49) 6131-39-25605. E-mail: tremel@uni-mainz.de.

[†] Institut für Anorganische Chemie und Analytische Chemie der Johannes Gutenberg-Universität.

[†] Institut für Physikalische Chemie der Johannes Gutenberg-Universität.

(1) Kroto, H. W.; Heath, J. R.; O'Brien, S. C.; Curl, R. F.; Smalley, R. E. *Nature* **1985**, *318*, 162–163.
(2) Lijima, S.; Toshinari, P.; Ando, Y. *Nature* **1992**, *356*, 776–778.
(3) Ugarte, D. *Science* **1991**, *359*, 707–709.
(4) Tenne, R.; Margulis, L.; Genut, M.; Hodes, G. *Nature* **1992**, *360*, 444–446.
(5) Remskar, M.; Mrzel, A.; Skraba, Z.; Jesih, A.; Ceh, M.; Demšar, J.; Stadelmann, P.; Levy, F.; Mihailovic, D. *Science* **2001**, *292*, 479–481.
(6) Rosenfeld-Hacohen, R.; Grunbaum, E.; Tenne, R.; Sloan, J.; Hutchison, J. L. *Nature* **1998**, *395*, 336–337.
(7) Peng, H. S.; Meister, S.; Chan, C. K.; Zhang, X. F.; Cui, Y. *Nano Lett.* **2007**, *7*, 199–203.
(8) Margulis, L.; Salitra, G.; Tenne, R.; Talianker, M. *Nature* **1993**, *365*, 113–114.
(9) (a) Feldman, Y.; Frey, G. L.; Homyonfer, M.; Lyakhovitskaya, V.; Margulis, L.; Cohen, H.; Hodes, G.; Hutchison, J. L.; Tenne, R. *J. Am. Chem. Soc.* **1996**, *118*, 5362–5367. (b) Feldman, Y.; Margulis, L.; Homyonfer, M.; Tenne, R. *High Temp. Mater. Processes* **1996**, *15*, 163–169. (c) Feldman, Y.; Zak, A.; Popovitz-Biro, R.; Tenne, R. *Solid State Sci.* **2000**, *2*, 663–672. (d) Li, X. L.; Li, Y. D. *Chem.—Eur. J.* **2003**, *9*, 2726–2731. (e) Zak, A.; Feldman, Y.; Alperovich, V.; Rosentsveig, R.; Tenne, R. *J. Am. Chem. Soc.* **2000**, *122*, 11108–11116. (f) Rothschild, A.; Tenne, R.; Sloan, J.; York, A. P. E.; Green, M. L. H.; Sloan, J.; Hutchison, J. L. *Chem. Commun.* **1999**, 363–364. (g) Schuffenhauer, C.; Popovitz-Biro, R.; Tenne, R. *J. Mater. Chem.* **2002**, *12*, 1587–1591.
(10) (a) Tsirlina, T.; Feldman, Y.; Homyonfer, M.; Sloan, J.; Hutchison, J. L.; Tenne, R. *Fullurene Sci. Technol.* **1998**, *6*, 157–165. (b) Whitby, R. L. D.; Hsu, W. K.; Lee, T. H.; Boothroyd, C. B.; Kroto, H. W.; Walton, D. R. M. *Chem. Phys. Lett.* **2002**, *359*, 68–76. (c) Coleman, K. S.; Sloan, J.; Hanson, N. A.; Brown, G.; Clancy, G. P.; Terrones, M.; Terrones, H.; Green, M. L. H. *J. Am. Chem. Soc.* **2002**, *124*, 11580–11581. (d) Margolin, A.; Popovitz-Biro, R.; Albu-Yaron, A.; Moshkovich, A.; Rapoport, L.; Tenne, R. *Curr. Nanosci.* **2005**, *1*, 253–262. (e) Yella, A.; Therese, A. H.; Zink, N.; Panthöfer, M.; Tremel, W. *Chem. Mater.* **2008**, *20*, 3587–3593.

10.1021/cm900277j CCC: $40.75
Published on Web 05/08/2009

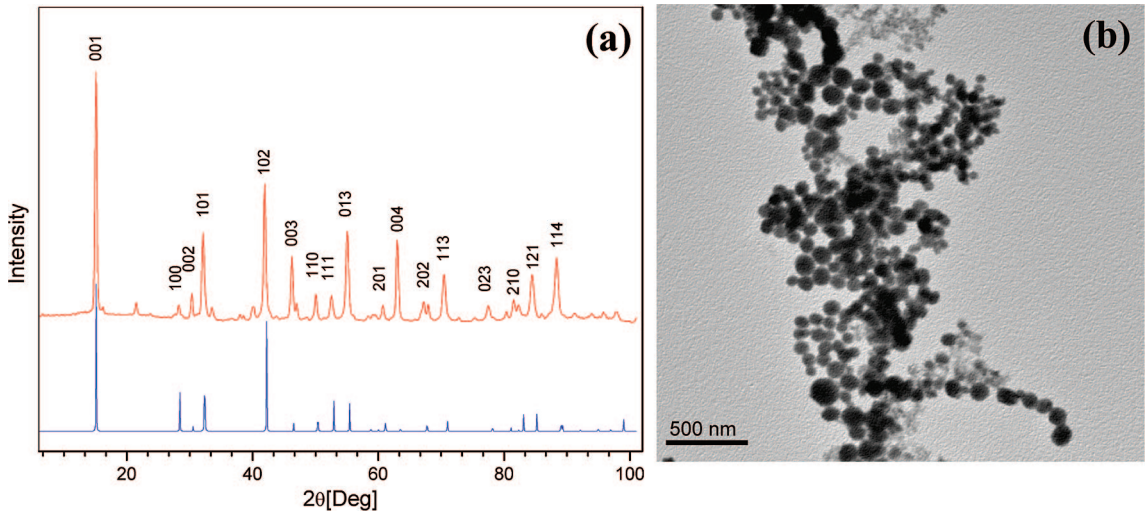

Figure 1. (a) X-ray powder diffraction pattern of the product obtained at 850 °C. The blue lines correspond to Berndtite-SnS_2. (b) Overview of the TEM image of the product obtained.

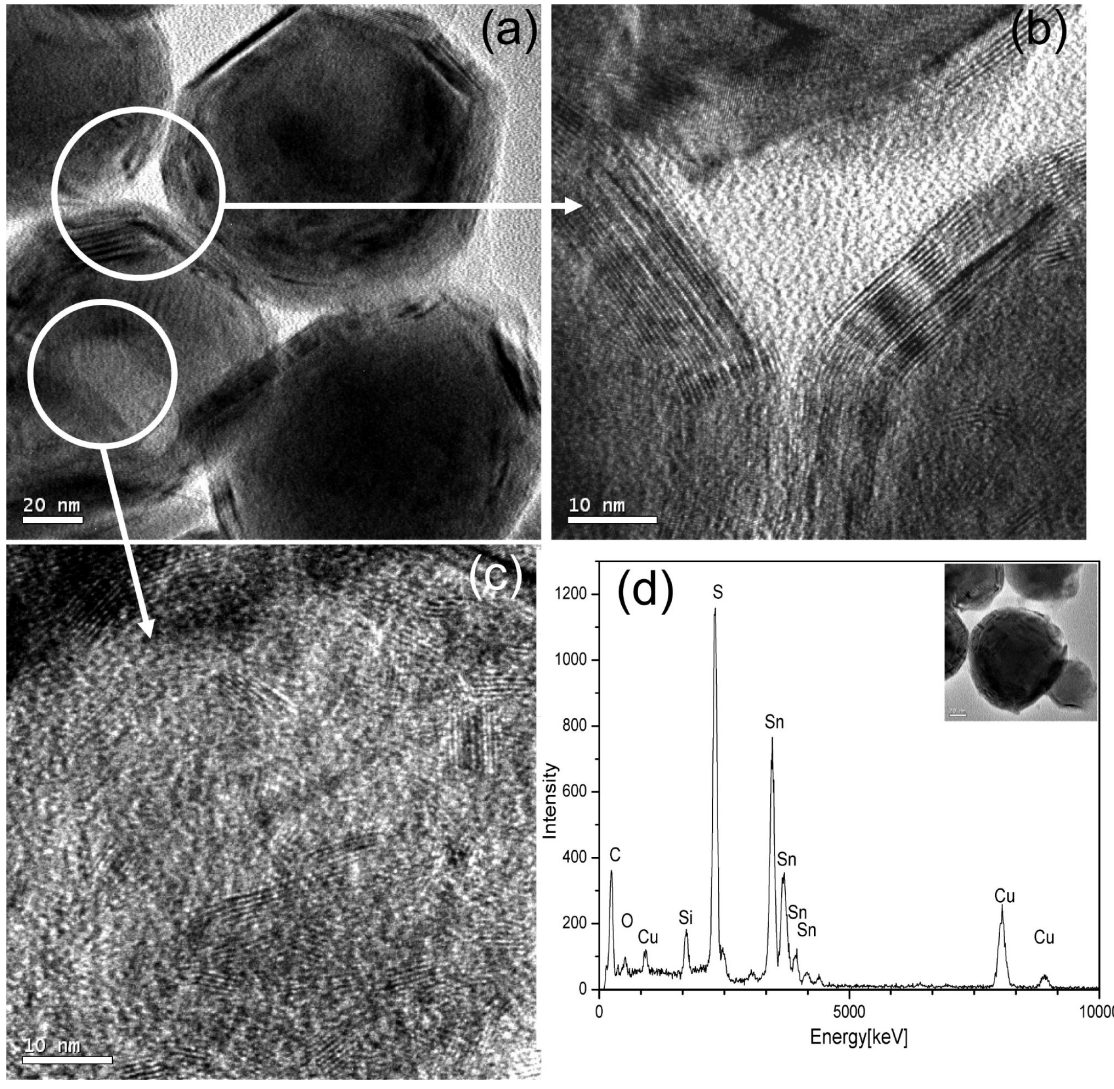

Figure 2. HRTEM image of (a) fullerene-like particles, (b) enlarged part of the rectangular region in a, (c) grain boundaries and amorphous domains in the circular region with in the particle; (d) EDX of the corresponding inset.

corresponding metal oxides with high oxidation states exist. Alternative synthetic approaches have made use of MOCVD[15] and APCVD,[16] chemical vapor transport,[5,17,18] or the thermal decomposition of sulfur-rich compounds.[19]

Tin disulfide adopts the layered CdI_2 structure type, in which the tin atoms are located in octahedral voids between two close packed slabs of sulfur to form a three-atom layered sandwich structure.[20] SnS_2, a lamellar semiconductor with a

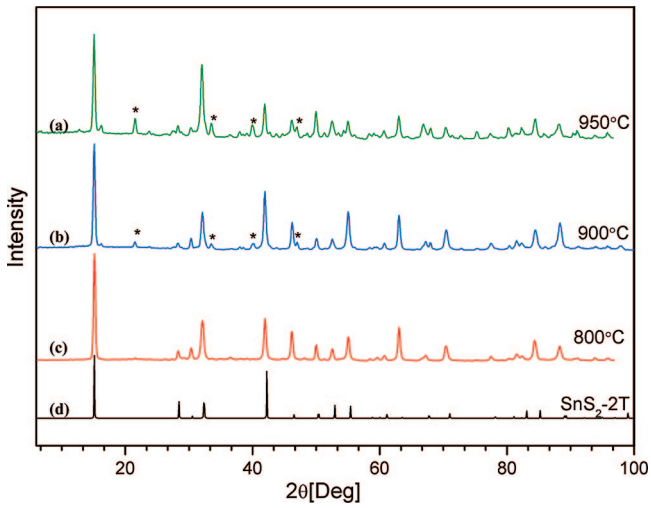

Figure 3. X-ray powder pattern of the products obtained at (a) 950, (b) 900, and (c) 800 °C, and (d) calculated pattern for Bernditite-1T SnS_2. Reflections marked with asterisk (*) correspond to Ottemannite (Sn_2S_3), the amount of which increases with increasing reaction temperature.

band gap of around 2.35 eV,[21] has attracted attention for its semiconducting properties and can potentially be used as an efficient solar cell material.[22] It is also of interest in holographic recording systems and electrical switching.[23] Recently, IF-SnS_{2-x} nanoparticles were obtained by laser ablation.[24] Many of these nanoparticles showed semiperiodic intensity alterations pointing to a misfit layer structure[25] of SnS_2 and layered SnS[26] with different periodicities. Here, we report a single-step process for the synthesis of SnS_2 fullerene-like nanoparticles, Sn/S/C composite dumbbells, SnS_2 nanotubes and SnS_2 nanoscrolls by a vapor transport technique. We also found that the sulfidizing agent CS_2 can act as a precursor for the growth of the carbon fibers.

Experimental Section

The synthesis of tin disulfide nanostructures was carried out in concentrically arranged quartz glass tubes that were heated in a horizontal tube furnace. One quartz tube is placed inside another one and the outer quartz tube has an inner/outer diameter of 35/30 mm and a length of 90 cm. The inner quartz tube had an inner/outer diameter of 24/20 mm and a length of 70 cm. The source material, bulk Sn grains of 99.9% purity (Aldrich), was first cleaned with HCl solution for 20 min to remove the surface oxide layer and subsequently placed in a quartz boat in the middle of the inner quartz tube. Argon gas was flushed through the tube for about half an hour to remove the air present. The furnace was heated to a temperature of 850 °C with a heating rate of 5 °C per min under Ar or Ar/CS_2 mixtures depending upon the conditions. After heating the furnace to the required temperature, an Ar/CS_2 mixture was passed through the tin melt at a flow rate of 300 mL/min for duration of 2 h. After the end of the reaction, the furnace was cooled to ambient temperature at a rate of 3 °C per min. The yellow product was obtained at the downstream end of the furnace from the outer tube at a temperature zone of 150−200 °C and collected with a spatula.

Characterization. *Electron Microscopy.* The products were characterized using high-resolution scanning electron microscopy (HRSEM) (LEO 1530 Field emission SEM, 6 kV extraction voltage). Transmission electron microscopy (TEM) was carried out on a Philips EM420 instrument at an accelerating voltage of 100 kV with a twin lens and a Philips CM12 with a twin lens at an acceleration voltage of 120 kV. High-resolution images were taken with a Philips FEI TECNAI F30 ST electron microscope (field-emission gun, 300 kV extraction voltage) equipped with an Oxford EDX (energy-dispersive X-ray) spectrometer with a Si/Li detector and an ultrathin window for elemental analysis. Image analysis and Fourier transform calculations were performed with Gatan Digital Micrograph software. Samples for TEM measurements were prepared from ethanolic suspensions of the samples. Three drops of the ultrasonicated suspension were administered on a Cu grid coated with FORMVAR polymer and an amorphous carbon layer.

X-ray Powder Diffraction. X-ray diffraction patterns (XRD) were recorded using a Bruker AXS D8 Discover powder microdiffractometer (Cu Kα radiation, graphite monochromator) equipped with a 2D HiStar detector. Phase analysis was performed using AXS Bruker EVA 10.0.[27]

Results and Discussion

The powderlike SnS_2 collected from the low-temperature region of the furnace appears yellow. The composition of the product was determined by X-ray powder diffraction (XRD). Most of the diffraction peaks of the as prepared nanoparticles could be attributed to Berndtite (SnS_2, JCPDS card no. 21−1231) with small contaminations from Ottemannite (Sn_2S_3) as shown in Figure 1a. The morphology can be seen in the TEM image in Figure 1b. Overall the product consists of round (IF)-like particles. Generally, particle sizes are in the range from 40 to 100 nm.

Structural information of the product was obtained from HRTEM and the corresponding energy-dispersive X-ray

(11) Therese, H. A.; Rocker, F.; Reiber, A.; Li, J.; Stepputat, M.; Glasser, G.; Kolb, U.; Tremel, W. *Angew. Chem.* **2005**, *117*, 267−270; *Angew. Chem., Int. Ed.* **2005**, *44*, 262−265.
(12) Therese, H. A.; Zink, N.; Kolb, U.; Tremel, W. *Solid State Sci.* **2006**, *8*, 1133–1135.
(13) Therese, H. A.; Li, J.; Kolb, U.; Tremel, W. *Solid State Sci.* **2005**, *7*, 67–72.
(14) Coleman, K. S.; Sloan, J.; Hanson, N. A.; Brown, G.; Clancy, G. P.; Terrones, M.; Terrones, H.; Green, M. L. H. *J. Am. Chem. Soc.* **2002**, *124*, 11580–11581.
(15) Etzkorn, J.; Therese, H. A.; Rocker, F.; Berntsen, N.; Schermann, W.; Kolb, U.; Tremel, W. *Adv. Mater.* **2005**, *17*, 2372–2375.
(16) (a) Vollath, D.; Szabo, D. V. *Acta Mater.* **2000**, *48*, 953–957. (b) Lee, G. H.; Jeong, J. W.; Huh, S. H.; Kim, C.; Kim, B. J.; Y. W, *Int. J. Mod. Phys. B* **2003**, *17*, 1134–1140.
(17) Nath, M.; Kar, S.; Raychaudhuri, A. K.; Rao, C. N. R. *Chem. Phys. Lett.* **2003**, *368*, 690–695.
(18) (a) Remskar, M.; Virsek, M.; Jesih, A. *Nano Lett.* **2008**, *8*, 76–80. (b) Remskar, M.; Mrzel, A.; Virsek, M.; Jesih, A. *Adv. Mater.* **2007**, *19*, 4276–4278.
(19) (a) Zelenski, C. M.; Dorhout, P. K. *J. Am. Chem. Soc.* **1998**, *120*, 734–742. (b) Chen, J.; Li, S. L.; Gao, F.; Tao, Z. L. *Chem. Mater.* **2003**, *15*, 1012–1015. (c) Nath, M.; Rao, C. N. R. *Chem. Commun.* **2001**, 2236–2237.
(20) (a) Fong, C. Y.; Cohen, M. L. *Phys. Rev. B* **1972**, *5*, 3095–3101. (b) Domingo, G.; Itoga, R. S.; Kannewurf, C. R. *Phys. Rev.* **1966**, *143*, 536–541.
(21) Lokhande, C. D. *J. Phys. D: Appl.Phys.* **1990**, *23*, 1703–1705.
(22) Loferski, J. J. *J. Appl. Phys.* **1956**, *27*, 777–784.
(23) (a) Chu, J.; Walser, R. M.; Bene, R. W.; Courtney, T. H. *Appl. Phys. Lett.* **1974**, *24*, 479–481. (b) Patil, S. G.; Fredgold, R. H. *J. Pure Appl. Phys.* **1971**, *4*, 718–720.
(24) Hong, S. Y.; Popovitz-Biro, R.; Prior, Y.; Tenne, R. *J. Am. Chem. Soc.* **2003**, *125*, 10470–10474.
(25) (a) Gomez-Herrero, A.; Landa-Canovas, A. R.; Hansen, S.; Otero-Diaz, L. C. *Micron* **2000**, *31*, 587–595. (b) Bernaerts, D.; Amelinckx, S.; Van Tendeloo, G.; Van Landuyt, J. *J. Cryst. Growth* **1997**, *172*, 433–439.
(26) Tremel, W.; Hoffmann, R. *Inorg. Chem.* **1987**, *26*, 118–128.
(27) *EVA 10.0*; Bruker AXS: Madison, WI, 2004.

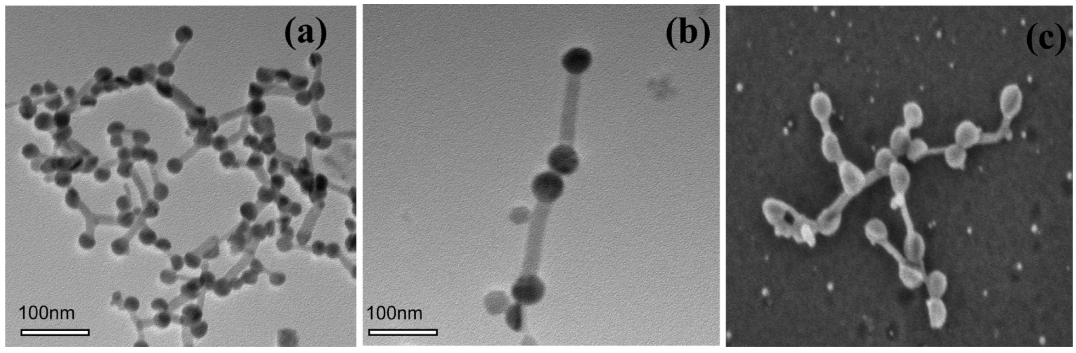

Figure 4. (a) Overview image of the product obtained at 1000 °C after 3 h of sulfidization. (b) Two dumbbells connected to each other. (c) SEM image of the nanocomposite.

spectroscopy (EDX) analysis (Figure 2). HRTEM shows that the product consists of closed-cage nanoparticles with both spherical and faceted morphologies. Both polyhedra are nested, i.e., closed multilayer nanostructures as shown in Figure 2. Varying the tilt angle of the sample in the TEM did not reveal any significant changes. Typical particle sizes were about 50−70 nm with a fairly narrow size distribution. A representative HRTEM image shows clear fringes with a separation of 0.59 nm, in good agreement with the interlayer spacing of the SnS_2. No hollow particles were observed. Some HRTEM images revealed the presence of remnant elemental tin (see Figure S1 in the Supporting Information) within the core of the particles indicating that the particles had not been completely sulfidized. Furthermore, some grain boundaries and amorphous domains were present in the core of the particles as shown in Figure 2c.

The composition of the core and the outer part of the IF-particles were examined by EDX analysis. The Sn:S ratio is close to 1:2 for the outer part and about 1:1.5 for the core which might be due to an incomplete sulfidization of the tin nanoparticles already formed because of vapor transport while heating. The Cu peaks arise from the TEM grid and the Si peak comes from the pole pieces of the microscope.

The formation of the SnS_2 fullerenes occurs by sulfidization of tin nanoparticles formed by vapor transport. Incomplete sulfidization due to sulfur depletion and/or slow sulfur diffusion through the SnS_2 mantle may lead to the formation of lower tin sulfides (Sn_2S_3 and SnS) or Sn remnants in the particle core. To elucidate the mechanism of the formation of the fullerene like particles, the conditions for the synthesis of tin disulfide were studied systematically in a series of experiments where the CS_2 gas flow rate, the reaction temperature, the duration of sulfidization, and the sulfidization delay time, i.e. the heating time before the sulfidization was started by allowing CS_2 to pass through the reaction furnace.

(a) Flow Rate of CS_2. The effect of the CS_2 gas flow rates was studied by varying the flow rates between 200 and 500 mL/min. With a reduced gas flow of 200−300 mL/min, mainly platelets of SnS_2, a few tens of nanometres to 0.5 μm in size were obtained. For higher flow rates (400−500 mL/min), mainly spherical particles with diameters of about 50 nm were obtained, while the amount of the of SnS_2 platelets was reduced. For flow rates above 500 mL/min, small spherical particles of SnS_2 were obtained. This is compatible with a trapping of IF-SnS_2 by dilution and quenching.

(b) Temperature. The temperature of the tube furnace was varied from 700−950 °C in steps of 100 °C during a set of experiments. In all experiments a yellow product was formed at the downstream end of the furnace (where the temperature was 150−200 °C). No difference in the particle size was observed when the temperature was changed from 700−950 °C while keeping the reaction time and the gas flow rate constant. The yield of the yellow product increases with increasing reaction temperature. In all cases, the product was formed in the low-temperature zone (150 °C < T < 150−200 °C). Although the particle size is almost the same in all cases, the amorphous domains present in the core of the fullerene-like particles transformed to Sn_2S_3 upon increasing temperatures. This is supported by the X-ray powder diffraction pattern; with increasing temperature, the amount of the side product of the Ottemannite phase (Sn_2S_3) increases as shown in Figure 3.

In all three cases, Berndtite (1T-SnS_2) was the dominant phase, but with increasing temperature, the amorphous domains present in the core of the nanoparticles transformed to Sn_2S_3. As the role of temperature seems to be less significant for the particle size, the temperature of the reaction zone was kept at 850 °C for the following experiments unless specified otherwise.

(c) Sulfidization Time. In a third set of experiments, the duration of the sulfidization reaction was varied from 2 to 6 h in steps of 1 h. For a constant gas flow of 400 mL/min an increase of the reaction times from 2 to 4 h at 850 °C resulted in the formation of smaller spherical particles (see Figure S2 in the Supporting Information). The nanoparticles do not grow further as the product is collected from the temperature zone of 150−200 °C. A possible reason for the smaller particle size with the increase in the duration of sulfidisation might be that the transport of Sn/S species due to their solubility in the gas phase (Ar carrier gas) becomes more important in a sense that material depletion in the gas phase sets a limit to the particle growth.

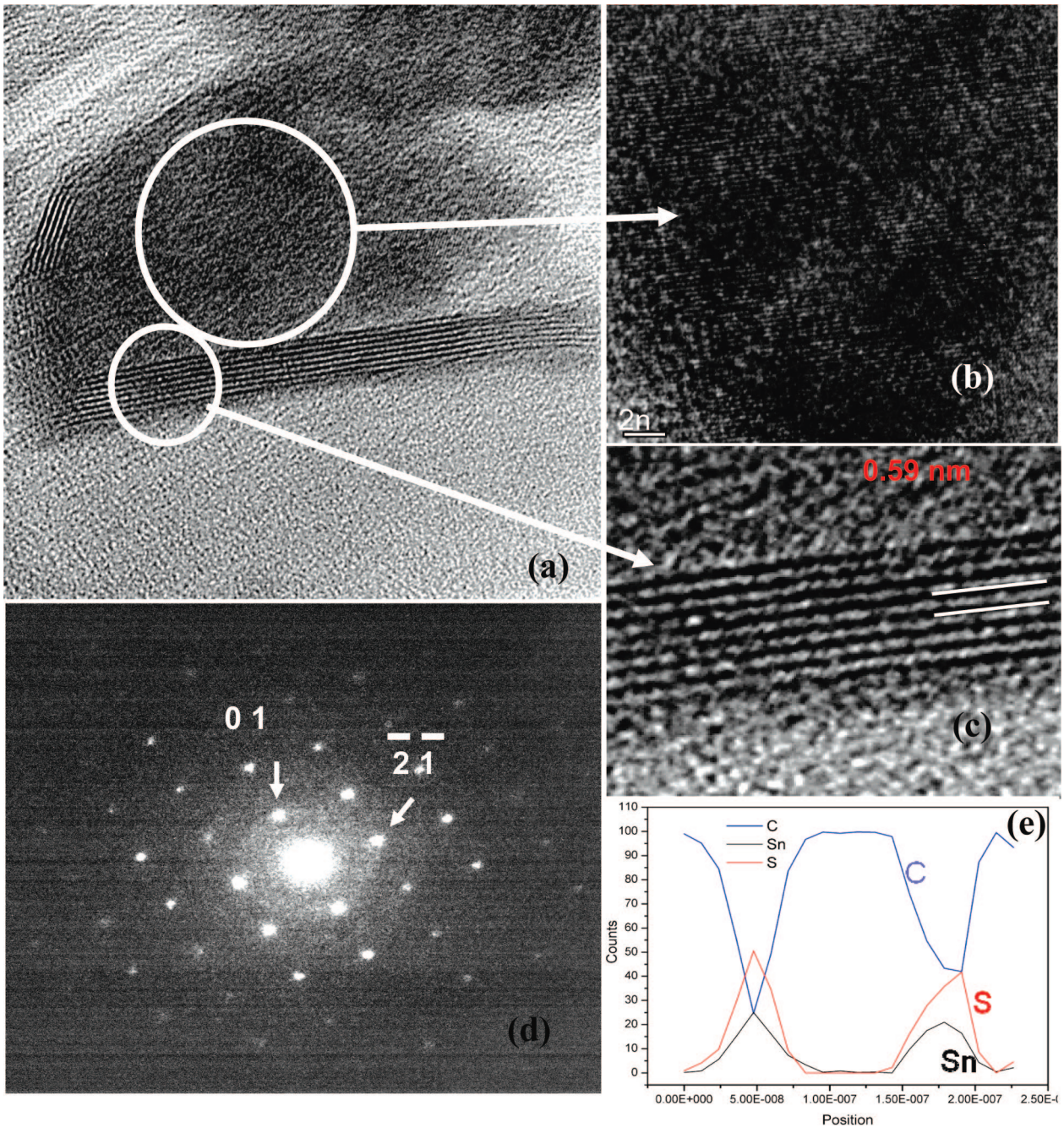

Figure 5. HRTEM image of Sn/S/C dumbbell shaped nanoparticles obtained after 3 h of sulfidization at 1000 °C. (a) HRTEM image of a round edge particle in dumbbells with a well-developed layered edge. (b) Enlarged view of the core, which matches with Sn_2S_3. (c) Enlarged view of layered rim with an interplanar distance of 0.59 nm (corresponding to SnS_2 (001) *d*-value). (d) NED pattern of a core of a round particle in dumbbells, all reflections can be indexed according to Sn_2S_3. HRTEM image of a particle core. (e) EDX line scan along the dumbbell shows that the round tips consists of Sn and S, whereas the axis connecting the round tips consists of C.

Interestingly, a prolonged reaction time up to 3.5 h at a temperature of 1000 °C resulted in the formation of composite Sn/S/C composite dumbbells as shown in Figure 4. HRTEM images of the composite dumbbells (Figure 5) show incomplete edges consisting of well-developed layers and cores characterized by a weaker contrast, but fully crystalline (Figure 5a−c). The layered edges are always present and an interplanar distance of 0.59 nm is consistent with a (001) lattice plane separation of SnS_2 (Figure 5c). Nanobeam electron diffraction (NED) patterns from the core show patterns consistent with the Ottemannite phase(Figure 5d). In most cases, the core consists of few intergrowth domains with different orientations. EDX on the round particles shows the presence of both, tin and sulfur. The high sulfur background prevents an accurate elemental quantification, but the Sn/S ratio is significantly higher in regions with higher number of crystalline layers.

Thus, the round particles of the dumbbells were found to be a mixture of SnS_2 and Sn_2S_3. Layered SnS_2 with a layer distance of 0.59 nm in the high resolution TEM is present only at the rim of the round particle. Sn_2S_3 is predominantly present in the core, as confirmed from the FFTs and NEDs. The axis connecting the round particles is amorphous and the line scan along the dumbbell shows that the axis is composed of carbon as shown in Figure 5e. The formation of amorphous carbon fibers might be attributed to fact that

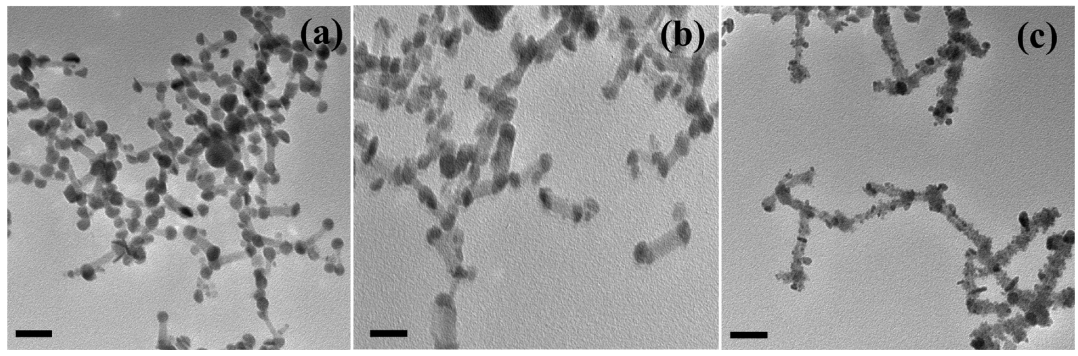

Figure 6. TEM images of the Sn/S/C nanocomposites obtained at 1000 °C at a duration of sulfidization reactions of (a) 5, (b) 6, and (c) 10 h. All the scale bars are 100 nm.

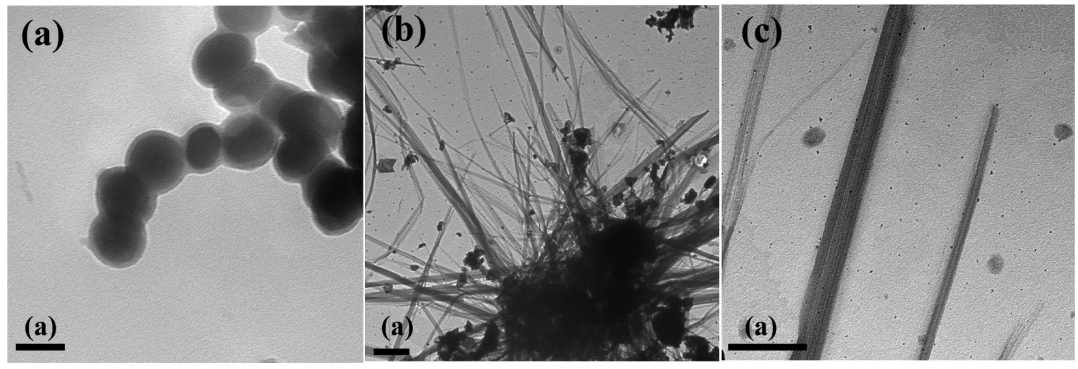

Figure 7. (a) TEM images of Sn@carbon core−shell nanoparticles obtained with cyclohexane as the carbon source, (b) TEM images obtained when 90% argon and 10% methane gas mixture was used as the carbon source, (c) more magnified TEM image of the amorphous carbon fibers in b.

tin acts as a catalyst in the formation of tin filled and/or hollow carbon nanotubes.[27] Thermal decomposition of CS_2 at 1000 °C and a rapid deposition of carbon species in the gas phase on the newly formed tin sulfide nanoparticles might be responsible for the formation of the composite nanodumbbells of Sn/S/C.

Extending the duration of the sulfidization to 5 and 6 h, did not lead to an increase in the length of the carbon fibers, but the diameter of the round Sn/S particles decreased instead. With a further increase in the duration of sulfidization to 10 h, the round particles completely vanished and much smaller particles of Sn/S, decorated onto the amorphous carbon fiber, were formed. The formation of carbon fiber with constant lengths even upon increasing the concentration of the gas phase carbon species by increasing the duration of sulfidization with CS_2 indicates that the growth of the carbon fibers has stopped at some point.

A possible explanation is that the growth of the carbon fibers and the sulfidization of the tin metal nanoparticles occur simultaneously. At some point, the sulfidization of the tin nanoparticles is complete, and hence the growth of the carbon fiber stops. As the transport of the Sn/S species due to their solubility in the gas phase (Ar carrier gas) becomes more important at these reaction temperatures, prolonged duration of the sulfidization at 1000 °C resulted in the product decomposition and the formation of smaller particles as shown in Figure 6c.

To elucidate the mechanism of the formation of the Sn/S/C nanocomposites, attempts are made to synthesize dumbbells of tin and carbon using carbon sources (cyclohexane and methane) other than CS_2, which resulted in the formation of different types of nanostructures. When CS_2 was replaced by cyclohexane, tin nanoparticles that were uniformly coated with a carbon mantle (thickness 5−7 nm) were obtained as shown in Figure 7. When 90% argon and 10% methane gas mixture was used, amorphous carbon fibers with a length of several micrometers were obtained ($T = 150-200$ °C) along with some amount of tin nanoparticles. Surprisingly, tin particles were not attached to the amorphous carbon fibers in contrast to a previously reported synthesis of carbon nanotubes using a tin catalyst.[27]

Thus, the formation of the dumbbell like Sn/S/C nanocomposites seems to be a result of the simultaneous sulfidization of the tin nanoparticles and the growth of the carbon fibers from the reaction CS_2 gas.

(d) Delay Time. Finally, the influence of the delay time (the heating time before the sulfidization was started by allowing CS_2 to pass through the reaction furnace) was studied. When CS_2 was supplied only after the reaction temperature had been reached, tin nanoparticles were formed by evaporation of tin metal powder and transported by the carrier gas to the colder zone of the furnace, where they were sulfidized. This reaction leads to the formation of IF-SnS_2 nanoparticles. However, when a sulfur source is already present when tin metal reaches a sufficiently large concentration in the gas phase at 850 °C, SnS_2 nanoscrolls and some nanosheets were obtained after 2 h as shown in the Figure 8.

A small amount of SnS_2 nanotubes were also present when the reaction was performed at 1000 °C. Nanosheets and nanoscrolls shown in Figure 8 have similar dimensions. This suggests that the nanoscrolls were formed from the sheets. When the reaction time was reduced from 2 h to 15 min,

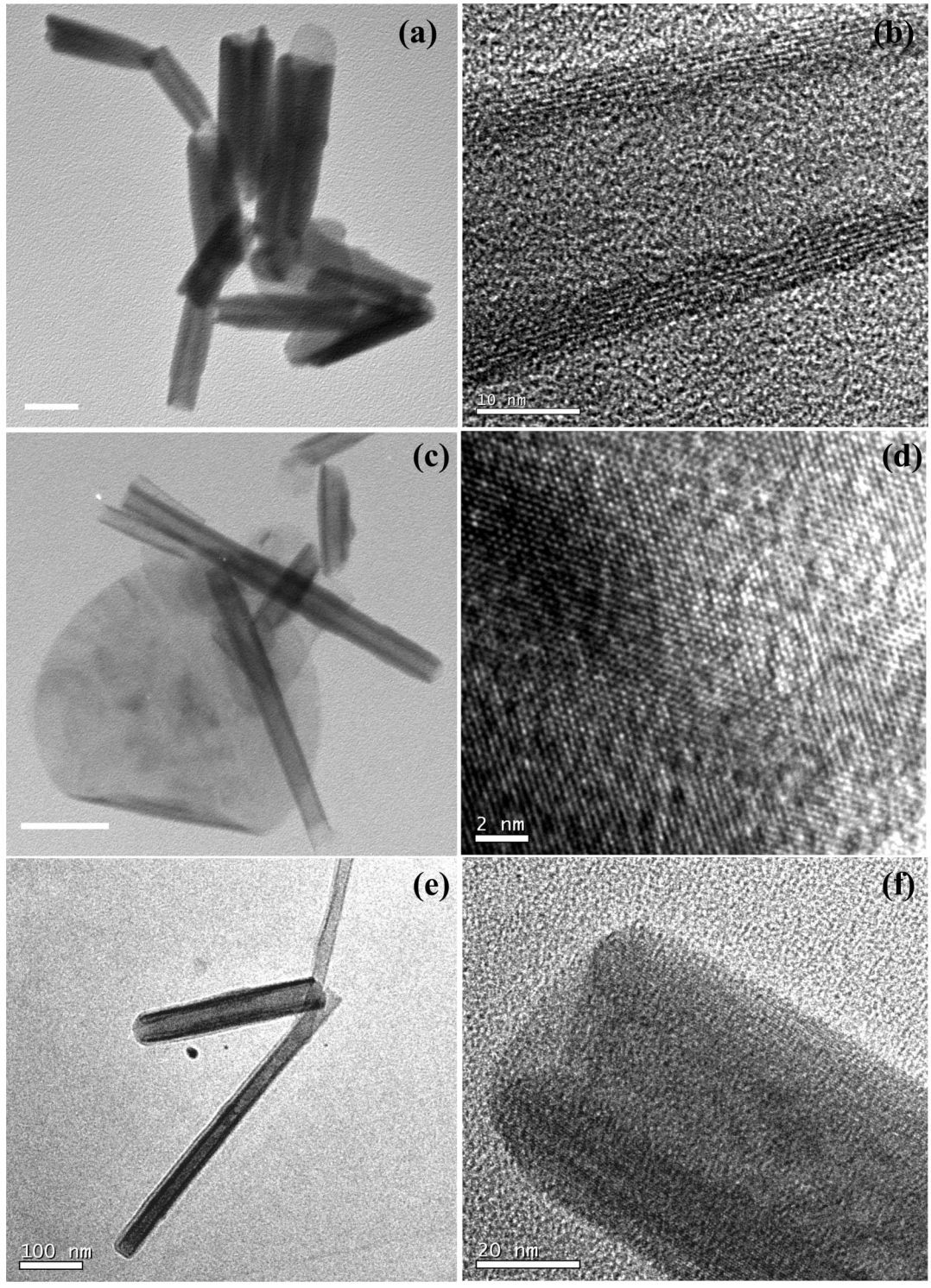

Figure 8. (a) Scrolls of SnS_2 obtained by feeding the Ar/CS_2 reaction gas while heating the tin metal powder; (b) HRTEM image of a scroll; (c) TEM image of a sheet scrolling; (d) HRTEM image of a sheet of SnS_2; (e) TEM image of nanotube of SnS_2 obtained at 1000 °C; and (f) HRTEM image of an open end of nanotube.

the yield of the nanosheets increases at the expense of the yield of the scrolls. On the other hand, when the nanosheets were isolated and subsequently annealed under argon at 200 and 300 °C for 30 min, no scrolling was observed, and agglomerated sheets of SnS_2 were formed instead. Thus a separation of the nanosheets in the gas phase seems to be necessary for the formation and stabilization of scrolls/tubes (low gas-phase concentration) by suppressing the formation of agglomerated bulk particles.

Conclusions

In summary, we have demonstrated a new and facile synthetic approach to nearly stoichiometric fullerene-like IF-SnS_2 nanoparticles that are difficult to obtain by other methods such as MOCVD or by the reductive sulfidization of the corresponding metal oxide, SnO_2. By varying the reaction conditions, particles with different morphologies such as fullerene-type particles, nanotubes, and composite SnS_2/C dumbbells were obtained. By

carefully controlling the reaction conditions these metastable phases can selectively be synthesized. This facile one-step approach may be up scaled easily for the synthesis of nanostructured SnS_2 in larger quantities. There are further prospects for analyzing the solid-state transformation of nanosheets into nanotubes of SnS_2 by in situ heating TEM studies.[28] Experiments toward this goal are in progress.

(28) (a) Cario, L.; Palvadeau, P.; Lafond, A.; Deudon, C.; Moelo, Y.; Corraze, B.; Meerschaut, A. *Chem. Mater.* **2003**, *15*, 943–950. (b) Rouxel, J.; Meerschaut, A.; Wiegers, G. A. *J. Alloys Compd.* **1995**, *229*, 144–157. (c) Wang, Y.; Lee, J. M. *Angew. Chem., Int. Ed.* **2006**, *45*, 7039–7042. (d) Prem Kumar., T.; Ramesh, R.; Lin, Y. Y.; Kuo Fey, G. T. *Electrochem. Commun.* **2004**, *6*, 520–525.

Acknowledgment. We acknowledge Mrs. S. Hartmann for help in the HRTEM analysis and Mr. G. Glasser (MPI-P) and Dr. M. N. Tahir for the SEM. This research was supported by a fellowship to A.Y. from POLYMAT, the Graduate School of Excellence of the State of Rhineland-Palatinate. We are indebted for support from the Materials Science Center (MWFZ) in Mainz and the Deutsche Forschungsgemeinschaft (DFG) under the auspices of SPP 1165.

Supporting Information Available: Additional images (PDF). This material is available free of charge via the Internet at http://pubs.acs.org.

CM900277J